Effect of Pulse On-Time and Peak Current Density on Pulse Plated Re-Ni Alloys

Tzippora Nusbaum,[a] Brian A. Rosen,[a,*,z] Eliezer Gileadi,[b,] and Noam Eliaz[a,***]**

[a]Department of Materials Science and Engineering, Faculty of Engineering, Tel Aviv University, Ramat Aviv 6997801, Israel
[b]School of Chemistry, Faculty of Exact Sciences, Tel Aviv University, Ramat Aviv 6997801, Israel

Rhenium (Re), with its unique chemical and mechanical properties, has sparked a rising interest in many communities in recent years. Electrochemical deposition has proven to be a promising method for the manufacture of Re-based products, with pulse electrodeposition allowing for finer control of the deposit properties. In this work, the effects of a wide range of pulse-plating parameters on the composition and microstructure of Re-Ni alloys were studied. The samples were examined under a scanning electron microscope, and it was found that a nodular morphology was generated in all samples within the region of pulse parameters investigated. A surface morphology diagram was constructed, delineating the conditions leading to colonies that extend perpendicularly from the substrate vs. those that remain nearly flat on the substrate surface ('rough' vs. 'smooth' deposits, respectively). XPS analysis showed an increase in the rhenium oxide content relative to pure Re, both at higher on-times and at higher peak current densities. XRD analysis showed that all samples contained fcc Ni, although certain fcc Ni reflections were absent in the case of smooth samples. This absence was coupled with evidence of a solid solution of Re in an hcp Ni lattice, found exclusively in the smooth samples.
© 2015 The Electrochemical Society. [DOI: 10.1149/2.0111507jes] All rights reserved.

Rhenium (Re) is known for its exceptional tolerance to extreme temperatures, high modulus of elasticity (exceeded only by Ir and Os), high shear modulus and excellent wear properties. It has been shown to be resistant to hydrochloric acid and seawater corrosion, and displays resistance to hydrogen and inert atmospheres at elevated temperatures.[1,2] As a result of these properties, the aerospace, nuclear, electrical, catalysis, and biomedical communities have become increasingly interested in utilizing Re for various applications in their respective fields.[3] Although much research focuses on the manufacture of Re-coatings via chemical vapor deposition (CVD), this process has proven to be costly, energy-inefficient, and produces coatings prone to delamination.[2] There is therefore a rising interest in electrochemical deposition of Re and its alloys, as electrodeposition offers a wide variety of parameters for controlling the properties of the resultant deposits. Deposits of pure Re are difficult to produce electrochemically from aqueous solutions due to the low overpotential for hydrogen evolution.[2] It has been found that the addition of an iron-group metal (Ni, Fe, Co) to the electroplating bath increases both the rate of Re deposition and the faradaic efficiency (FE),[4–7] and leads to significantly less brittle coatings.

Pulse electrodeposition offers many advantages over traditional direct-current (DC) electroplating. It provides additional free variables to control the physics of the deposition process, including peak current density (j_p), pulse on-time (t_{on}), and pulse off-time (t_{off}).[8,9] Pulse plating can therefore be used to create electrodeposits with compositions, morphologies, and microstructures unattainable by DC plating for three main reasons:[8]

- Through replenishment of the diffusion layer during t_{off}, pulse electrodeposition allows for a higher instantaneous current density by creating a steeper concentration gradient.
- The high overpotentials made possible by pulse electrodeposition increase the available energy for nuclei formation, and therefore higher nucleation rates are attainable with pulses, as compared to DC plating. Pulse electrodeposition can therefore be used to produce coatings with finer grains.
- During t_{off}, electroless adsorption, desorption, and recrystallization reactions can occur on the surface as a result of relaxation at the interface.

Despite these benefits, only few papers in the literature have focused on pulse plating of rhenium alloys.[10,11] Our goal is to explore the effects of t_{on} and j_p on the surface morphology, microstructure and composition of Re-Ni alloys, as well as to investigate how the electrochemical parameters influence changes in deposit characteristics.

Experimental

A jacketed 40 ml three-electrode electrochemical cell was used for all deposition experiments. The working electrode (WE) was a copper disk with an exposed surface area of 1.57 cm^2. The two counter electrodes (CE) were platinum gauzes (mesh size 52) placed 5 mm on either side of the WE. Each WE was cleaned just before electroplating by immersion for 1 min in a 1:1 volumetric mixture of nitric acid (70% HNO$_3$/H$_2$O) : deionized (DI) water at room temperature. Prior to deposition, the electrodes were rinsed with DI water, dried in air, and weighed. The reference electrode was Ag/AgCl/KCl(sat). The electrolyte contained 450 mM nickel (II) sulfamate tetrahydrate, 225 mM citric acid, and 10 mM ammonium perrhenate, adjusted to a pH of 5.0 ± 0.2 with concentrated sodium hydroxide. The concentrations of the metal ions in solution were chosen such that perrhenate reduction was mass-transport controlled and nickel deposition was activation controlled. As a result, only the concentration gradient of the perrhenate diffusion-layer was sensitive to the pulse parameters. By contrast, the nickel ion concentration was large enough that its concentration resembled the bulk regardless of pulsing.[11,12] Previous research in our group showed that for dilute Ni electrolytes, a nickel-to-citrate ratio of 2:1 yields the highest FE for DC plating.[13] We therefore used the same ratio in an effort to maximize the efficiency of our deposition. Pulse plating was carried out using a Bio-Logic VSP potentiostat/galvanostat, controlled by EC-Lab software. A thermostatic bath was used to maintain the electrolyte temperature of 40 ± 1°C, and the electrolyte was stirred by a magnetic bar.

For all experiments, a total charge of 10 C/cm^2 was passed, and the t_{off} was 30 ms. The current density during all off-times was –0.05 mA cm^{-2} in order to prevent inadvertent oxidation[c]. The electrolyte was purged with nitrogen gas at about 200 standard cubic centimeters per minute (sccm) for 30 minutes prior to each experiment. Likewise, the headspace of the cell was purged with nitrogen gas during experiments in order to minimize the concentration of oxygen in the solution during electroplating.

The surface morphology of the coating was evaluated using a scanning electron microscope (SEM) operated in high-vacuum mode (Quanta 200 FEG from FEI). Compositional analysis was carried out
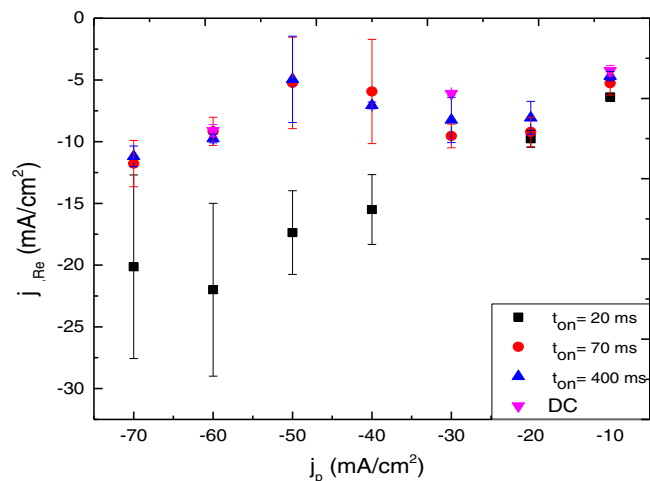
---

*Electrochemical Society Student Member.
**Electrochemical Society Fellow.
***Electrochemical Society Active Member.
zE-mail: barosen@post.tau.ac.il

c Although strictly speaking a current density of –0.05 mA cm^{-2} does not constitute off-time per-se, we shall refer to these conditions as "off time" hereafter, since negligible current was flowing through the system.
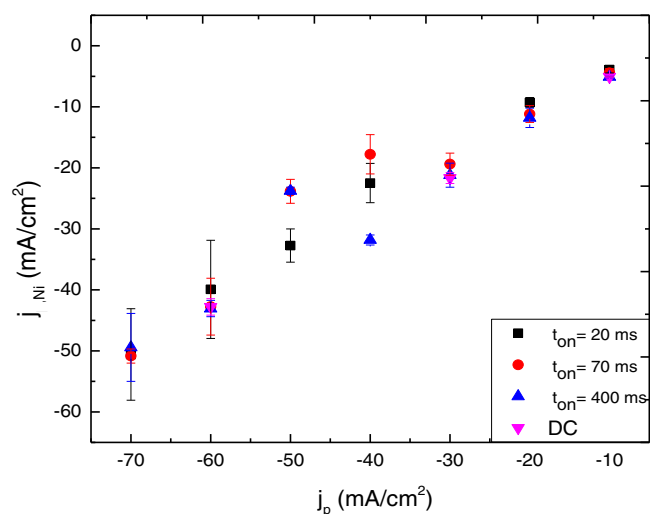
**Figure 1.** Partial current density of Re vs. peak current density.

using energy-dispersive spectroscopy (EDS) with a liquid-nitrogen-cooled Oxford SI detector attached to the SEM. SEM and EDS analyses were conducted at 6–11 different locations on each coating, in order to ensure accuracy of the values obtained. Crystallographic measurements were taken using X-ray diffraction (XRD). The diffractometer (Scintag, USA) was equipped with a liquid-nitrogen-cooled Ge solid-state detector and a Cu K_α radiation source. Information about the oxidation states of Re was obtained by means of X-ray photoelectron spectroscopy (XPS), using a 5600 Multi-Technique system (PHI, USA) operating in ultrahigh vacuum. The samples were irradiated with an Al K_α monochromatic source, and the electrons were analyzed by a Spherical Capacitor Analyzer with a split aperture of 0.8 mm. The C1 peak at 285 eV was taken as the energy reference for all measured peaks and samples. A charge neutralizer was used for charge compensation due to carbon accumulation on the surface of some samples. The FE was calculated using Equation 1 from the mass of the deposit, the chemical composition of the alloy (determined by EDS), and the total charge passed in each experiment:

$$FE = w(It)^{-1} \sum c_i n_i F(m_i)^{-1} \cdot 100 \qquad [1]$$

where w is the added mass of the deposit, I is the total current passed, t is the deposition time, c_i is the weight fraction of the element (Re or Ni), n_i is the number of electrons transferred per atom for each metal (7 for Re, 2 for Ni), F is Faraday's constant (96485 C mol^{-1}), and m_i is the atomic mass of the metal (186.2 g mol^{-1} for Re and 58.71

Figure 2. Partial current density of Ni vs. peak current density.
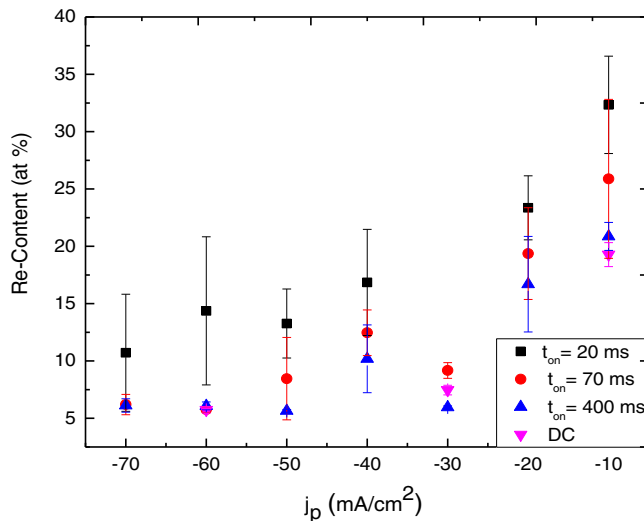
Figure 3. Re-content in the deposit as a function of peak current density.

g mol^{-1} for Ni). It should be noted that the calculated FE does not take into account the rhenium oxides found in XPS analysis. This is due to the fact that the Re-oxides are assumed to be formed via the spontaneous decomposition of rhenium hydride upon exposure of the deposit to air after electrodeposition (or in solution, while no potential is applied). If so, the contribution of the oxides to the deposit weight is insignificant in comparison to that of metallic rhenium.

Results and Discussion

The pulse electrodeposition of Re-Ni alloys on copper substrates was studied at various on-times and peak current densities. The effect of these parameters on the partial current densities of Re and Ni (partial current densities of Re and Ni section), faradaic efficiency (faradaic efficiency section), and surface morphology and microstructure of the coatings (surface morphology and microstructure section) are considered.

Partial current densities of Re and Ni.— A comparison of the partial current density of Re ($j_{,Re}$) vs. applied peak current density (Figure 1) shows that for on-times at and above 70 ms, $j_{,Re}$ remains relatively low and closely resembles that of DC experiments[d]. The partial current density for component i is defined by Equation 2:

$$j_i = \frac{w}{t} \frac{c_i n_i F}{m_i} \qquad [2]$$

At $t_{on} = 20$ ms, however, $j_{,Re}$ increases dramatically due to the steep perrhenate concentration gradient generated as a result of the pulsing. The concentrations of ReO_4^- and Ni^{2+} in solution were chosen to ensure that within the parameters of our experiment, the deposition of Re will be mass-transport controlled and Ni will be activation-controlled. The linear relation between the partial current density of Ni ($j_{,Ni}$) and j_p, shown in Figure 2, confirms our description of Ni as being virtually unaffected by the pulse parameters. The exclusive effect of the increased concentration gradient on rhenium rather than nickel is further demonstrated by considering the concentration of Re in the deposit, shown in Figure 3. While the Re-content in the deposit barely changes at high current densities (above 30 mA cm^{-2}) and on-times above 70 ms (including DC), a sharp rise is noted at low current densities and short on-times. This rise can be attributed to perrhenate ion replenishment at sufficiently short on-times. Additionally, it has been shown[2,14] that in the case of binary alloy deposition, the less noble metal (in this case Ni) is preferentially deposited at higher overpotentials. This is clearly demonstrated by the drop in Re-content in the alloy for larger values of j_p (higher overpotentials).
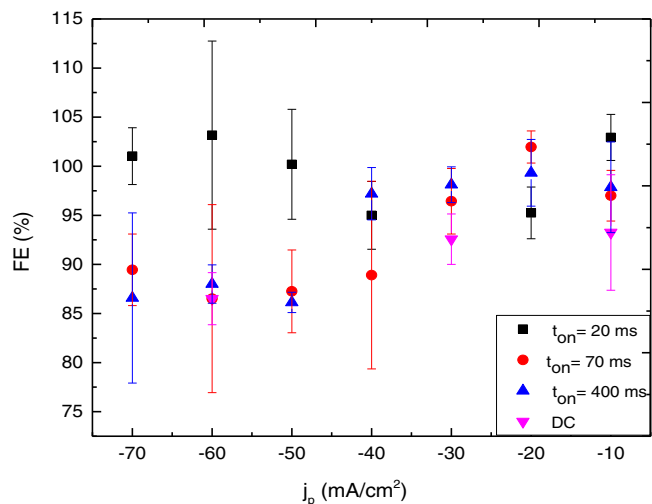
Figure 4. Faradaic efficiency vs. peak current density.

Faradaic efficiency.— In Figure 4, the calculated FE is plotted against the applied peak current density. The FE for the DC samples falls by nearly 15% as the current density becomes more cathodic, suggesting that the DC limiting current density (j_{lim}) is being surpassed. The same drop in FE is observed for pulse plated samples at on-times above 70 ms, suggesting that on-times above 70 ms gen-

erate surfaces resembling their DC analogs. In DC electrodeposition (or pulse electrodeposition parameters resembling DC conditions), the FE will drop when the average current density, j_{avg}, exceeds the limiting current density, j_{lim}, due to the appearance of unwanted side reactions (e.g. hydrogen evolution). Therefore, a FE of 100% can only be achieved if the condition in Equation 3 is satisfied:[9]

$$j_p t_{on}(t_{pp})^{-1} = j_p \theta = j_{avg} \leq j_{lim} \qquad [3]$$

where t_{pp} is the total pulse time and θ is the duty cycle $\{t_{on}(t_{on} + t_{off})^{-1}\}$. From Equation 3 it follows that an increase in either the on-time or the peak current density leads to an increase in j_{avg}. In systems where pulsing gives rise to changes in the diffusion layer profile of the electroactive species (at on-times below 70 ms in our work), the limiting current density is instead characterized by the pulse limiting current density, j_{pL}, which takes into account the transient effects of the pulsating diffusion layer not described by the j_{lim} variable. The pulse limiting current density represents the current density for which the surface concentration of electroactive species equals zero at the end of a pulse. The drop in FE at on-times of 70 ms and above and current densities over –30 mA cm^{-2} suggests that under these conditions, the applied peak current density exceeds j_{pL} (c.f. Refs. 8 and 15). Some data points and error bars in Figure 4 exceed a faradaic efficiency of 100%. This may be due to experimental error, which would likely be eliminated by increasing the number of times the experiment is repeated ($n = 3$). An alternative cause for the observed FE > 100% may be electroless deposition by metallic nickel. Berkh et al. noted
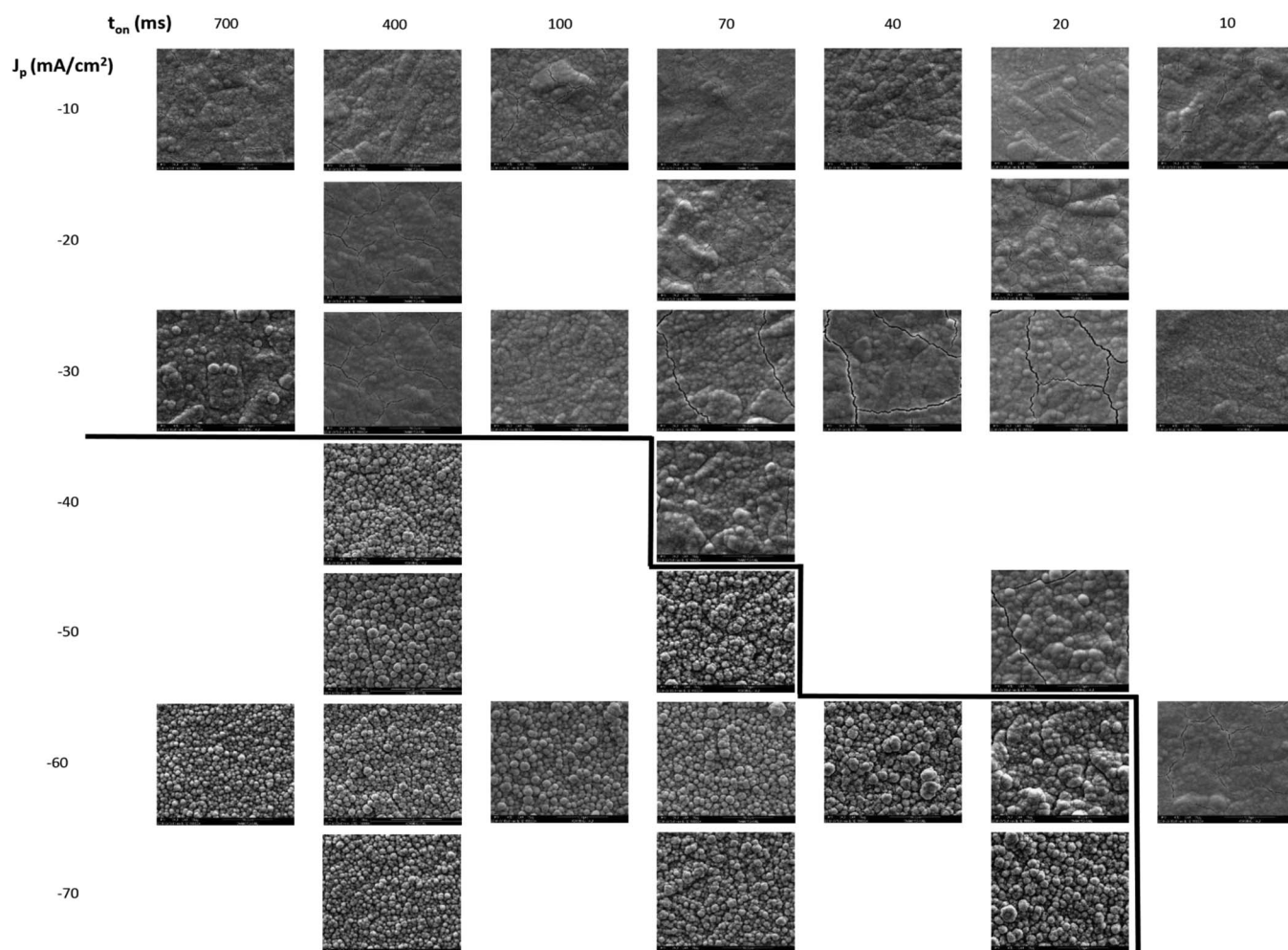
Figure 5. Surface morphologies obtained for the range of pulse parameters studied. Each column represents a series of experiments conducted at constant on-times. Every row is a series of experiments at constant peak current densities. The step-shaped line approximates the transition from smooth to rough topography.
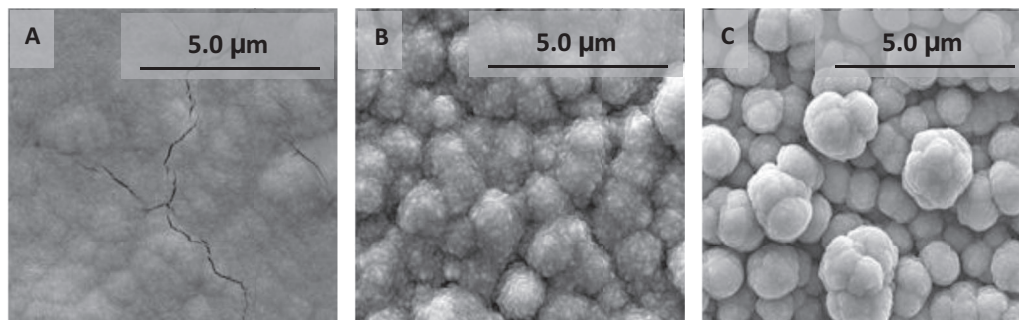
Figure 6. SEM images of coatings from DC plating at (a) –10 mA cm^{-2}, (b) –30 mA cm^{-2}, and (c) –60 mA cm^{-2}.

a similar phenomenon in their research, albeit at significantly higher faradaic efficiencies.[6,7]

Surface morphology and microstructure.— Figure 5 contains a table summarizing the full range of morphologies observed in this study. Each column in the table represents a series of experiments conducted at a constant on-time (ranging from 10 to 700 ms). Each row represents a series of experiments at a constant peak current density (ranging from –10 to –70 mA cm^{-2}). The nodular morphology observed is known as a "mesoscale colony structure", and each colony is comprised of nano-sized grains with similar crystallographic orientation separated by low-angle boundaries.[16,17] Studies of Ni-W coatings suggest that the circular/quasi-circular nature of the colonies may allude to the total absence of grain boundaries.[18,19] Coatings produced at $j_p = -10$, –20, and –30 mA cm^{-2}, at all values of t_{on} considered in this study (10 to 700 ms) remained relatively flat on the substrate surface, and will be referred to hereafter as "smooth." On the other hand, experiments conducted at both high values of j_p and long values of t_{on} produced coatings whose colonies extend perpendicularly from the substrate surface, and will be referred to hereafter as "rough." The step-shaped line in Figure 5 approximates the surface morphology transition from smooth to rough. ImageJ software was used to estimate the surface roughness based on contrast analysis of the 2D SEM images. Thus, we could estimate a roughly 150% increase in surface roughness from "smooth" to "rough" samples.

For comparative purposes, Figures 6a–6c show coatings generated under DC conditions at –10, –30, and –60 mA cm^{-2}, respectively. Ibl comments that at long on-times, pulse systems begin to mimic DC conditions,[8] as verified by Figures 5 and 6.

A surface morphology diagram (current density vs. t_{on}) is presented in Figure 7. Three distinct regions can be observed:

(I) Low peak current densities (below –30 mA cm^{-2}) where smooth coatings are produced regardless of the on-time, since j_{lim} ($\approx j_{pL}$) is not exceeded.

(II) An intermediate zone in which smooth deposits are produced despite having surpassed j_{lim}, as long as j_{pL} is not exceeded.

(III) Long on-times coupled with high peak current densities, at which rough coatings are always produced because j_{pL} is exceeded.

The three regions of the surface morphology diagram may be understood in light of the DC (j_{lim}) and pulse limited current densities (j_{pL}). In Region I, the applied peak current density falls below j_{lim}, resulting in deposition with high values of FE and smooth deposits. In Region II, the system has surpassed j_{lim}, however higher limiting current densities are allowed due to pulsing. In this region, smooth samples are still observed up until j_{pL} at which point the FE drops and rough samples are obtained. This is therefore a clear demonstration of the higher instantaneous current densities achievable by pulse as opposed to DC electrodeposition. In Region III, the applied current density exceeds j_{pL}, leading to competing reactions and a corresponding drop in FE. The issue of hydrogen evolution is particularly relevant in Re-Ni alloys, both because Re has a low hydrogen overpotential and

because hydrogen bubbles tend to cling to Ni surfaces without necessarily being absorbed into the coating.[2,20] These adsorbed bubbles then inhibit uniform metal deposition that would ordinarily produce smooth coatings, as metal ions deposit around the hydrogen bubbles, rather than directly onto the surface.[21] El-Sherik et al. reported that where severe hydrogen-bubble clinging was observed, "pitted" surfaces were formed. This is in contrast to the smooth deposits generated in their experiments with negligible hydrogen clinging.[21]

Increase of the applied current density will increase the hydrogen overpotential,[20] as is indeed observed in the rough coatings produced at higher current densities (Figures 5 and 7). It should be mentioned that other factors such as the alloying metal, substrate, pH, and temperature will also affect the rate of hydrogen evolution,[20] however all such parameters were held constant in our experiments and are therefore assumed not to be the root cause of the morphological differences observed.

Additionally, El-Sherik et al. reported that hydrogen production was enhanced at longer on-times, consistent with our observations. Longer on-times allow more time for diffusion layer growth and subsequent depletion of metal cations adjacent to the surface. As our system is galvanostatic, the depletion of metal ions will necessarily lead to side reactions such as hydrogen evolution. The co-evolution of hydrogen as a result of transient metal depletion can therefore explain the trend of rougher coatings produced at longer values of t_{on} (Figures 5 and 7). Pulse plating can therefore act as a method to control hydrogen evolution and the subsequent morphology of Ni-Re coatings as the pulse off-time will replenish the diffusion layer with metal ions.

It is interesting to note that there are inherent difficulties in modeling j_{pL} or measuring j_{lim} for the present system, since the hydrodynamics are difficult to model in a multi-component parallel plate system when a magnetic stir bar is used. The results presented in
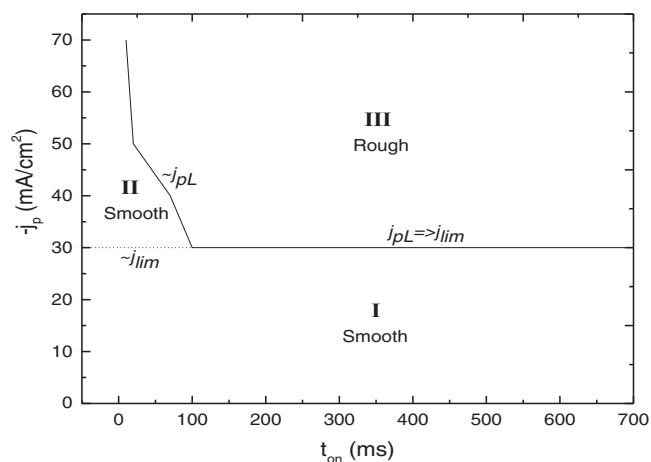
Figure 7. Surface morphology diagram constructed based on the morphologies observed under SEM.

Table I. Pulse parameters for samples analyzed by XPS and XRD.

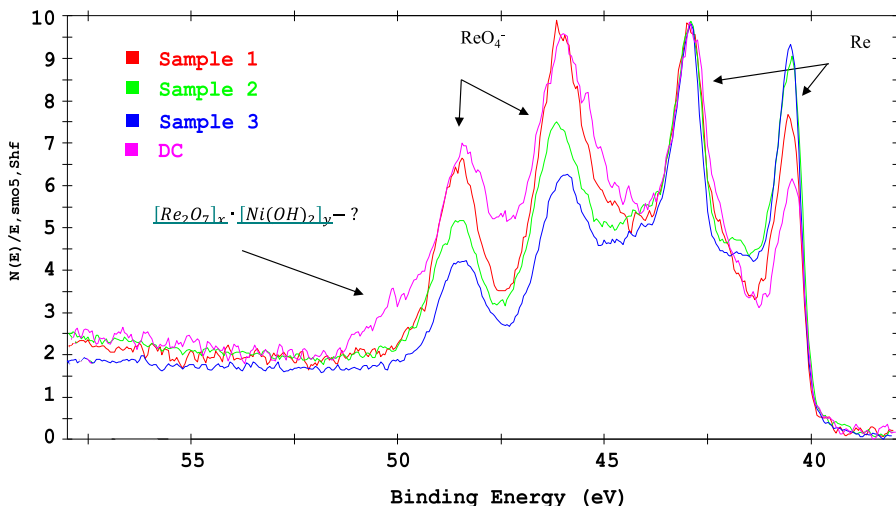| Sample	Morphology	j_p (mA cm^{-2})	t_{on} (ms)
1	rough	−60	400
2	smooth	−20	400
3	smooth	−60	10
4	rough	−60	DC

Figures 4 and 5 allow for an approximation of both of these parameters by observing the onset of hydrogen evolution by monitoring the faradaic efficiency and the transition in surface morphology. We are therefore able to construct a morphology diagram in Figure 7 relating the morphology of our deposit to these parameters.

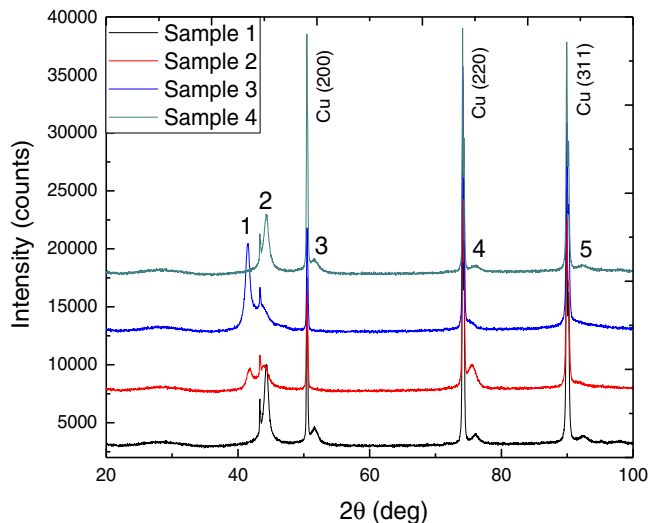## Microstructural and Chemical Analysis

Four characteristic samples, including three pulse-plated samples and one DC sample, were chosen for further analysis using XPS and XRD. The relevant pulse parameters are summarized in Table I.

The XPS spectra from all four samples are displayed in Figure 8. All spectra are composed mainly of rhenium oxides and metallic Re, while the DC sample contained evidence of an additional phase not present in any other coating. The position of the unknown peak suggests that this phase is either Re_2O_7, or a Re-Ni-oxide complex.[5] In the rough specimens (**Samples 1** and **4**), the metallic Re-content was half that of the Re oxides. In contrast, smooth specimens (**Samples 2** and **3**) contained approximately equal amounts of metallic Re and rhenium oxides. The increase in metallic Re-content relative to the oxides in smooth samples (when the on-time was shortened from 400 to 10 ms at a constant j_p) correlates well with the findings of Rosen et al.,[11] recently published by our laboratory. In that work, electrodeposition was carried out using an identical electrolyte as in our present experiments, however on a rotating cylinder electrode. Rhenium oxide formation was found to occur primarily during the pulse on-time, while the electroless reduction of the oxide phases (possibly to metallic Re) occurred primarily during t_{off}. It is therefore not surprising that as we decreased the duty cycle from 100% (DC) to 25% ($t_{on} = 10$ ms) at a constant current density, there is a corresponding strengthening of the Re peak relative to that of its oxide. This same reasoning explains the observed decrease in Re relative to the oxides when j_p is increased from −20 to −60 mA cm^{-2} at a constant t_{on}. Since the rhenium oxide formation occurs mainly during the pulse on-time, it follows that the higher the current density during t_{on}, the stronger the oxide peak observed.

Figure 9 shows the XRD spectra from the four samples analyzed. Peaks resulting from the copper substrate were not considered in our analysis. The peaks at 44.26° (Peak #2) and 75.40° (Peak #4)

Figure 9. XRD spectra. **Sample 1**: $j_p = −60$ mA cm^{-2}, $t_{on} = 400$ ms, **Sample 2**: $j_p = −20$ mA cm^{-2}, $t_{on} = 400$ ms, **Sample 3**: $j_p = −60$ mA cm^{-2}, $t_{on} = 10$ ms, **Sample 4**: DC, $j_p = −60$ mA cm^{-2}.

were identified in all four samples, albeit with varying intensities. These may correspond to the (111) and (220) planes of fcc nickel, respectively (JCPDS card #97-006-4989). Similarly, the peaks at 51.55° (Peak #3) and 92.23° (Peak #5) may correspond to the fcc nickel planes (200) and (311), respectively (JCPDS card #97-006-4989); however, they are present only in the rough specimens (**Samples 1** and **4**). The absence of (200) and (311) Ni reflections in the smooth specimens (**Samples 2** and **3**) is mirrored by a doubling of the Re-content (as measured by EDS) relative to the rough specimens (**Samples 1** and **4**). It is noteworthy that no evidence of (200) and (311) Ni reflections is found in the samples described in Rosen et al.,[11] all of which had smooth surface morphology and included at least twice the amount of Re than the rough samples discussed above.

Peak #1, centered at 41.74°, is seen only in **Samples 2** and **3** (both smooth). A similar peak was observed in our earlier work,[11] which was thought to correspond to a (002) plane of a solid solution of Re atoms included into an hcp-Ni lattice (JCPDS card #01-089-7129).[11,22,23] The doubling of the Re-content in **Samples 2** and **3** relative to **Samples 1** and **4** supports the suggestion that Peak #1 may correspond to a Re-Ni solid solution found exclusively in the smooth samples. Additionally, the appearance of *hcp*-Ni Peak #1 in **Samples 2** and **3**

Figure 8. HR-XPS spectra in the Re 4f region. **Sample 1**: $j_p = −60$ mA cm^{-2}, $t_{on} = 400$ ms, **Sample 2**: $j_p = −20$ mA cm^{-2}, $t_{on} = 400$ ms, **Sample 3**: $j_p = −60$ mA cm^{-2}, $t_{on} = 10$ ms, **Sample 4**: DC, $j_p = −60$ mA cm^{-2}.

may be linked to the absence of *fcc* Ni Peaks #3 and #5 in those same samples.

Further fitting of spectra 2 and 3 was impossible due both to the lack of Ni peaks corresponding to phases (200) and (311), and the potential evidence of (002) and (103) Re reflections (Peaks #1 and #4, respectively), see JCPDS card #01-071-4930.

Peaks #2, 3, 4, and 5 are all found 0.23°–0.98° more negative than the reference fcc nickel spectrum. This may allude to the presence of rhenium within the fcc-Ni lattice, since the atomic radius of Re is larger than that of Ni. The inconsistency in the extent of shift may be due to an uneven distribution of Re atoms within the fcc and hcp Ni phases.

Conclusions

The effects of a wide range of pulse-plating parameters on the composition and microstructure of Re-Ni alloys plated on copper disk electrodes were studied. The resulting surface morphology diagram may be divided into three regions: (I) Peak current densities below –30 mA cm^{-2}: Smooth coatings were produced for all tested on-times (10 to 700 ms), since $j_p < j_{lim}$. (II) $j_p = -30$ to -50 mA cm^{-2}, $t_{on} = 10$ to 100 ms: Since $j_{lim} < j_p < j_{pL}$, smooth coatings were observed, however increasing either j_p or t_{on} led to rough coatings. (III) Long on-times coupled with high peak current densities: $j_p > j_{pL}$, and therefore rough coatings were produced. When j_p exceeds j_{pL}, the system experiences increased hydrogen evolution, which may give rise to molecular hydrogen attached to the surface leading to rougher deposits.

In XPS analysis, it was found that the concentration of rhenium oxides decreases relative to that of Re when either the duty cycle or peak current density decreases. A similar trend was noted by Rosen et al.,[11] and is attributed to the formation of rhenium oxides primarily during t_{on}, as opposed to oxide reduction to metallic Re, which is an electroless process. The XRD spectra suggest that the fcc Ni planes (111) and (220) are present in all samples studied. fcc-Ni planes (200) and (311) were likewise found in rough samples, although there is no evidence of such phases in any of the smooth samples tested (including those reported by Rosen et al.).[11] The absence of *fcc* Ni reflections (200) and (311) in the smooth samples is accompanied by a doubling of the Re-content in these samples as compared with rough deposits. In addition, the smooth deposits contain evidence of a solid solution of Re in *hcp*-Ni. Rosen et al. noted a similar phase in their research, all of which was conducted on smooth deposits. These phenomena can be understood in light of the preferred Ni deposition at higher overpotentials (i.e. parameters producing rough coatings).

The relatively wide range of pulse parameters considered in this study provide useful information for the preparation of samples involving the electrodeposition of Re-Ni alloys for catalytic and other applications.

References

1. *ASM Handbook*, ASM International, Ohio (1990).
2. N. Eliaz and E. Gileadi, in *Modern Aspects of Electrochemistry*, p. 191, Springer, (2008).
3. A. Naor, N. Eliaz, E. Gileadi, and S. Taylor, *AMMTIAC Quarterly*, **5**, 11, (2010).
4. A. Naor, N. Eliaz, and E. Gileadi, *Journal of the Electrochemical Society*, **157**(7), D422 (2010).
5. A. Naor, N. Eliaz, L. Burstein, and E. Gileadi, *Electrochemical and Solid-State Letters*, **13**(12), D91 (2010).
6. O. Berkh, N. Eliaz, and E. Gileadi, *Journal of the Electrochemical Society*, **161**(5), D219 (2014).
7. O. Berkh, A. Khatchatouriants, N. Eliaz, and E. Gileadi, *Journal of the Electrochemical Society*, **161**(12), D632 (2014).
8. N. Ibl, *Surface Technology*, **10**(2), 81 (1980).
9. S. Roy and D. Landolt, *Journal of Applied Electrochemistry*, **27**(3), 299 (1997).
10. K. Hosokawa, H. Angerer, J. Puippe, and N. Ibl, *Plating and Surface Finishing*, **67**(10), 52 (1980).
11. B. A. Rosen, E. Gileadi, and N. Eliaz, *Journal of Electroanalytical Chemistry*, **731** 93 (2014).
12. A. Marlot, P. Kern, and D. Landolt, *Electrochimica Acta*, **48**(1), 29 (2002).
13. A. Naor, N. Eliaz, and E. Gileadi, *Electrochimica Acta*, **54**(25), 6028 (2009).
14. A. F. Jankowski, C. K. Saw, J. F. Harper, B. F. Vallier, J. L. Ferreira, and J. P. Hayes, *Thin Solid Films*, **494**(1), 268 (2006).
15. M. Datta and D. Landolt, *Surface technology*, **25**(2), 97 (1985).
16. S. Ruan and C. A. Schuh, *Journal of Materials Research*, **27**(12), 1638 (2012).
17. P. Cizek, M. Barnett, M. Nave, E. Rauch, and R. Balasubramaniam, *Metallurgical and Materials Transactions A*, **42**(7), 2048 (2011).
18. O. Younes, L. Zhu, Y. Rosenberg, Y. Shacham-Diamand, and E. Gileadi, *Langmuir*, **17**(26), 8270 (2001).
19. M. Farzaneh, K. Raeissi, and M. Golozar, *Journal of Alloys and Compounds*, **489**(2), 488 (2010).
20. D. Gabe, *Journal of Applied Electrochemistry*, **27**(8), 908 (1997).
21. A. El-Sherik, U. Erb, and J. Page, *Surface and Coatings Technology*, **88**(1), 70 (1997).
22. S. Pané, E. Pellicer, K. Sivaraman, S. Suriñach, M. Baró, B. Nelson, and J. Sort, *Electrochimica Acta*, **56**(24), 8979 (2011).
23. S. Pané, B. Özkale, K. Sivaraman, C. Ruiz-Camps, S. Suriñach, M. Baró, B. Nelson, J. Sort, and E. Pellicer, *Electrochimica Acta*, **96**, 43 (2013).